This is the peer-reviewed, final accepted version for American Mineralogist, published by the Mineralogical Society of America.
The published version is subject to change. Cite as Authors (Year) Title. American Mineralogist, in press.
DOI: https://doi.org/10.2138/am-2022-8162. http://www.minsocam.org/

Revision 2

Tracing structural relicts of the ikaite-to-calcite transformation in cryogenic cave glendonite

Péter Németh[1,2], Paul Töchterle[3], Yuri Dublyansky[3], Roland Stalder[4], Zsombor Molnár[2], Szilvia Klébert[5], Christoph Spötl[3]

[1] Institute for Geological and Geochemical Research, Research Centre for Astronomy and Earth Sciences, Eötvös Loránd Research Network, Budaörsi street 45, Budapest, 1112, Hungary

[2] Research Institute of Biomolecular and Chemical Engineering, University of Pannonia, Egyetem út 10, Veszprém, 8200, Hungary

[3] Institute of Geology, University of Innsbruck, Innrain 52, Innsbruck, Austria

[4] Institute of Mineralogy and Petrography, University of Innsbruck, Innrain 52, Innsbruck, Austria

[5] Institute of Materials and Environmental Chemistry, Research Centre for Natural Sciences, Magyar tudósok körútja 2, 1117 Budapest, Hungary

*Correspondence to: nemeth.peter@csfk.org

Key words
Ikaite, glendonite, cryogenic, calcite, TEM

This is the peer-reviewed, final accepted version for American Mineralogist, published by the Mineralogical Society of America.
The published version is subject to change. Cite as Authors (Year) Title. American Mineralogist, in press.
DOI: https://doi.org/10.2138/am-2022-8162. http://www.minsocam.org/

ABSTRACT

Ikaite is a calcium carbonate hexahydrate that forms at temperatures close to the freezing point of water, thus its occurrence is associated with cryogenic conditions. This mineral is metastable and quickly transforms to calcite at temperatures above 5 °C. Pseudomorphs of calcite after ikaite are known as glendonite. The nanostructure of 25,000-43,000 year-old glendonite from Victoria cave (Southern Ural, Russia) was investigated in search of structural features indicative of the ikaite-to-calcite transformation. Scanning electron microscope images display several μm to subμm-size pores and indicate high intergranular porosity among the loosely aggregated grains. Transmission electron microscopy (TEM) data show evidence of 10-20 nm nanotwins (twin law $(10\bar{1}4)$) and 10-40 nm overlapping nanograins. Scanning TEM images reveal that the individual grains contain 5-10 nm long and 2-4 nm wide mesopores (size between 2 and 50 nm), which are aligned parallel to $[10\bar{1}0]$ of calcite and might be associated with a crystallographically oriented dehydration of the precursor ikaite. Fourier transform infrared spectroscopy revealed no evidence of structural water but absorption bands related to molecular water trapped in fluid inclusions are present. Nitrogen absorption/desorption measurements show that the specific surface area of 5.78 m^2/g and the pore volume of ~0.07 cm^3/g for calcite, the constituent of glendonite, are comparable to those of a common natural calcite. We suggest that the aligned mesopores, frequently occurring twins, small grain size, presence of aqueous inclusions and the high μm to subμm-size intergranular porosity arise from the ikaite-to-calcite transformation and thus may be used as criteria for the former presence of ikaite and hence for cold paleotemperatures. However, since similar features might also be common in biogenic carbonates, the diagnostic macroscopic pseudomorphs after ikaite are equally important for identifying glendonites and inferring cryogenic conditions.

This is the peer-reviewed, final accepted version for American Mineralogist, published by the Mineralogical Society of America.
The published version is subject to change. Cite as Authors (Year) Title. American Mineralogist, in press.
DOI: https://doi.org/10.2138/am-2022-8162. http://www.minsocam.org/

INTRODUCTION

Ikaite (calcium carbonate hexahydrate) is a water-rich cryogenic mineral. Although it was already synthesized in the 19th century from a highly alkaline $Ca(OH)_2$ solution (Peluse 1865), its first natural occurrence was only reported almost a century later from submarine tufa columns in Ikka Fjord, Greenland (Pauly 1963). Since then it has been described from organic-rich deep-sea sediments (Suess et al. 1982; Jansen et al. 1987), alkaline lakes (Council and Bennett 1993) and ice caves (Onac et al. 2010; Bazarova et al. 2014). It has also been reported as a product of portlandite dissolution in concrete lining of cold riverbeds (Boch et al. 2015) as well as in speleothems associated with hyperalkaline groundwater originating from industrial lime-kilning processes (Field et al. 2017).

Ikaite formation is favored at cold conditions (< 5 °C), high pH (> 9) and in the presence of orthophosphates (Brooks et al. 1950; Hu et al. 2014). Anaerobic decomposition of organic matter was also reported to provide conditions favorable for ikaite formation (Greinert and Derkachev 2004). Ikaite formation at 7 °C reported by Field et al. (2017) may be a special case attributed to the hyperalkaline (pH > 12) environment of lime-kilning. In a laboratory setting ikaite has been synthesized even above 10 °C by increasing the concentration of orthophosphate and decreasing the CO_2 pressure (Brooks et al. 1950) as well as by increasing the Mg/Ca ratio of the parent solution (Purgstaller et al. 2017). Though ikaite formation was reported even at 35 °C (Tollefsen et al. 2020), naturally occurring ikaite is widely regarded as a reliable indicator for cold conditions.

The use of ikaite for inferring past cryogenic temperatures is challenging, because above 5 °C this mineral transforms to anhydrous $CaCO_3$, exclusively calcite in natural samples. This transformation involves the release of weakly bound water, present in the crystal structure of ikaite. In the latter the water molecules are bonded to $CaCO_3$ ion pairs and the neighboring ion pairs are connected via hydrogen bonds, which are very sensitive to temperature increase (Swainson and Hammond 2003, Demichelis et al. 2013). The controlling step in the process of ikaite transformation to calcite above 5 °C is the nucleation of anhydrous $CaCO_3$ and the concomitant release of water (Swainson and Hammond 2003). Macroscopic calcite pseudomorphs after ikaite are traditionally called glendonite, however, other names such as thinolite and pseudogaylussite have also been used (Hugget et al. 2005). These pseudomorphs have been reported from sedimentary rocks and have been interpreted as indicators of low paleotemperatures (Larsen, 1994; De Lurio and Frakes 1999), though Popov et al (2019) described glendonite occurrences from the Baltoscandian Basin and suggested significantly high paleotemperatures (>40°C) for the glendonite-bearing strata. The pseudomorphs preserve the original ikaite morphology, i.e. steep and spiky canted tetragonal pyramids (Fig. 1a, b, c). Swainson and Hammond (2001) showed that these forms uniquely define the precursor ikaite. Hugget et al. (2005)

investigated the petrography of calcite pseudomorphs after ikaite from several localities and found that the initial stage of ikaite decomposition was similar in all samples and involved the formation of a strongly zoned and dominantly fluid inclusion-rich rounded calcite core. However, the detailed nature of the transformation is still poorly understood due to the incomplete characterization of diagnostic microstructures (Reeder, 1992) of the calcite that formed in the space previously occupied by ikaite.

Here, we report unique microstructural features that could be associated with the ikaite-to-calcite transformation preserved in glendonite. We studied the crystal structure, water content and porosity of samples from Victoria cave (Southern Ural, Russia) and compared them with data reported for a natural and a synthetic calcite.

EXPERIMENTAL METHODS

Glendonite samples were collected in a hydrologically inactive passage of Victoria Cave (N 53.0490, E 57.0454, altitude 380 meter above sea level). The sampled deposit comprises glendonite intermixed with grains of cryogenic calcite, which yielded ^{230}Th/U ages between 25,000 and 43,000 years before present (Dublyansky et al. 2018). The modern mean cave air temperature is 5.6°C, which is greater than the mean annual air temperature outside the cave (0.9°C). The morphology of the samples was investigated with a Keyence VHX-5000 digital microscope. In order to document the texture of the pseudomorphs, samples were investigated using a JEOL JSM-6010LV scanning electron microscope (SEM). Samples were gold coated and secondary electron images were acquired using an acceleration voltage of 15 kV.

Glendonite from Victoria cave was crushed in ethanol using an agate mortar and deposited onto copper grids covered by Lacey carbon supporting films. According to Larsson and Christy (2008) such a preparation can induce deformation, although it is very unlikely that the observed $(10\bar{1}4)$ calcite twins were formed during grinding since the main deformation plane is $(01\bar{1}8)$ (Barber and Wenk 1979). High-resolution transmission electron microscopy (HRTEM), high-angle annular dark-field scanning TEM (HAADF-STEM) images and selected area electron diffraction (SAED) data were acquired with a 200 keV Talos Thermo Scientific electron microscope. In TEM mode the gun lens and the spot size were set to the nominal values of 4 and 6, respectively. SAED patterns were obtained with 520 mm camera length and a 0.2 μm size aperture. Energy dispersive X-ray spectra (EDS) were acquired with a "Super-X" detector system using four silicon drift detectors built into the microscope column. EDS data were obtained from a 100 x 100 μm size region. Fast Fourier transforms (FFTs) obtained from the HRTEM images were calculated using Gatan Digital Micrograph 3.6.1 software. VESTA-win64

111 software (Momma and Izumi 2011) was used to draw the structure models of ikaite and calcite. We
112 note that three independent indices *hkl* are used to label reflections and *d*-spacings and four indices *hkil*
113 ($i = -(h+k)$) whenever crystallographic planes and directions are discussed.
114 Another aliquot of the glendonite sample was ground lightly in an agate mortar to break up
115 aggregates for FTIR analyses. In order to discriminate between adhesive moisture and molecular water
116 hosted by fluid inclusions, a subsample was soaked in deuterium oxide (D_2O, 99.95 %; *Acros*
117 *Organics*) for 48 hours before measurements. This way, a partial exchange of adhesive H_2O by D_2O is
118 expected, while fluid inclusions should not be affected. The exchange of H_2O by D_2O is easily detected
119 by the respective OH and OD vibrations in the IR spectra. Unpolarized IR spectra of glendonite and
120 reference material were recorded at room temperature in transmission mode and in attenuated total
121 reflectance (ATR) mode using a Bruker Vertex 70 Fourier transform IR spectrometer equipped with a
122 liquid nitrogen-cooled MCT-detector, a globar light source and KBr beam splitter. Measurements were
123 performed with a spectral resolution of 2 cm^{-1} between 550 and 7500 cm^{-1} (transmission mode) and
124 between 600 and 5500 cm^{-1} (ATR-mode).
125 For documenting the pore characteristics and measuring the volume increase at equilibrium as a
126 function of the relative pressure, nitrogen physisorption experiments were performed at -196 °C using a
127 Quantachrome Autosorb 1C static volumetric apparatus. An untreated and a ground sample were
128 outgassed prior to measurements at 300 °C for 24 h under vacuum. The grinding was performed in an
129 agate mortar for three minutes. Adsorption data were obtained using ca. 0.15 g of sample and
130 successive doses of the selected gas until $p/p_0 = 1$ relative pressure was reached. The specific surface
131 area was calculated by the BET method (Brunauer et al. 1938) in the range of relative pressures from
132 0.1 to 0.33. The mesopore size distribution was calculated from the desorption branch of the isotherms
133 with the BJH method (Barrett et al. 1951).

134
135 ## RESULTS AND DISCUSSION

136 *Morphological characteristics of glendonite, chemical composition and pores*
137 Glendonite pseudomorphs have a complex structure comprising a moderately indurated sheath-like
138 outer "shell" and a somewhat less indurated clumpy "infill" (Fig. 1b). The overall "shell" morphology
139 conforms to that of the precursor ikaite crystals (canted tetragonal pyramid; Figs. 1b, c). Both "shell"
140 and "infill" are polycrystalline; composed of fine-grained (subμm to several μm-size grains) calcite
141 crystals. With rare exceptions (Figs. 1d, e), the crystals are anhedral. There are no signs of cementation;
142 the material is characterized by substantial inter-granular porosity (subμm to several μm-size pores;

Figs. 1d-g). The described glendonite pseudomorphs occur individually or are assembled in drusy aggregates (Fig. 1a).

Based on ICP-OES measurements Németh (2021) reported that the glendonite powder from Victoria cave contains 39.99 m% Ca and 0.045 m% Mg, i.e., the sample is practically pure $CaCO_3$. In order to study possible nanoscale chemical homogeneity, the intensity of HAADF-STEM images, also called Z contrast images, was used. As this parameter is directly related to the square of the atomic number, it provides information on chemical heterogeneity and nanoporosity if the composition and thickness of the particles are uniform. In the case of our glendonite, these images reveal several particles consisting of 50-200 nm size $CaCO_3$ nanocrystals that share the same crystallographic orientation (Fig. 2a), similar to what was previously reported for Mg-bearing calcite (Nyírő-Kósa et al. 2018). A characteristic feature of the HAADF images are 5-10 nm long and 2-4 nm thick grey intensity regions within the bright particles (Fig. 2b). Their fairly uniform intensity suggests that these regions are pores in the calcite. Following the International Union of Pure and Applied Chemistry (IUPAC) classification, these are mesopores (size between 2 and 50 nm). It is intriguing that these mesopores are aligned along <100> with respect to calcite (space group $R\bar{3}c$), and it is possible that they may arise from a crystallographically oriented dehydration of the precursor ikaite. In fact, the structure model of ikaite viewed along [010] indicates that the Ca atoms and the carbonate units are separated by water-rich layers parallel to the (001) plane (Fig. 2c). During transformation these water-rich layers may dehydrate leaving behind the observed [10-10] aligned mesopores in calcite. Supposing such a scenario a crystallographic orientation relationship between ikaite and calcite may be hypothesized (Figs. 2c, d). We stress, however, that the presence of aligned mesopores alone is not conclusive with respect to the crystallographic relationship. In fact, Tollefsen et al. (2020) reported that the pseudomorphic replacement of ikaite by calcite occurs via a coupled dissolution–reprecipitation mechanism at the ikaite–calcite interface. During this process the disappearance of the original crystallographic orientation of the precursor ikaite can be expected. Electron diffraction data of precursor ikaite and calcite are necessary in order to clarify these relationships.

$(10\bar{1}4)$ nanotwins in glendonite

The X-ray diffraction patterns of samples from Victoria cave are consistent with ordinary calcite (Németh 2021). No structural remnants of ikaite were found during TEM analysis. However, the HRTEM and SAED data reveal the occurrence of $(10\bar{1}4)$ nanotwins in glendonite. In particular, HRTEM images show sharp straight lines parallel to $(10\bar{1}4)$ that border domains and SAED patterns

reveal extra reflections halfway between those of calcite (Figs. 3a, b). Interestingly, these reflections match the so-called *c*-type reflections, which were previously attributed to various calcite superstructures and ordering (Reeder and Wenk 1979, Van Tendeloo et al. 1985). Larsson and Christy (2008), however, showed that these reflections could also arise from twins within a calcite matrix. This explanation is favored here because the *c*-type reflections occur in the practically chemically pure $CaCO_3$ glendonite sample (Fig. 2b). A detailed description of these $(10\bar{1}4)$ calcite twins, which could be misinterpreted as structural ordering, was recently reported in Németh (2021).

The estimated $(10\bar{1}4)$ twin domain size is ~5-20 nm (Figs. 3a, b). Moiré patterns and pseudo-lattice fringes with spacing an order of magnitude larger (thus, nm) than the original lattice spacings were also identified in HRTEM images (Figs. 3b, c, d). These images and the satellite reflections of the corresponding FFTs are indicative of the superpositions of 10-40 nm size nanograins. The $(10\bar{1}4)$ twins are commonly associated with crystal growth and have been reported among others from the calcite shell of a sea urchin (Larsson and Christy 2008). Our sample formed from ikaite, thus it is possible that the $(10\bar{1}4)$ twins are associated with the ikaite-to-calcite transformation. This process is accompanied by a large amount of water loss (50 mass %). Thus, the question arises whether there is any water still present inside the crystal structure.

Molecular water in glendonite

Besides the sharp absorption band characteristic of calcite, FTIR spectra of glendonite show a broad absorption band between wavenumbers 3100 and 3700 cm^{-1} (Fig. 4), indicating the presence of molecular H_2O. Organic molecules that contain O-H bonds could also cause absorption in this part of the spectrum, however, we can rule out their occurrence as the main and characteristic absorption bands indicative of organics are notably absent. Repeated measurements of D_2O-treated glendonites do not reveal a characteristic broad absorption band between 2200 and 2800 cm^{-1} that is indicative of D_2O. All absorption bands in this region can be attributed to calcite. The molecular water signal was not observed in ATR mode, where only roughly the outermost 0.5 μm of the sample are captured.

Given these observations, we infer that molecular H_2O is present in glendonite from Victoria cave. We interpret these data as evidence for the presence of nanometer-sized water-filled inclusions in calcite crystals that build up this glendonite sample. There is no evidence of structural water that is associated with relicts or partially dehydrated nano-domains of ikaite.

Porosity (low-temperature nitrogen adsorption)

SEM and TEM images (Figs. 1, 2) reveal a variety of inter- and intragranular pores. According to FTIR data (Fig. 4), some pores are filled with water. In order to quantify porosity and characterize the pore structure of glendonite, we performed nitrogen physisorption measurements. These measurements characterize the intragranular nanometer-size porosity of small calcite crystals which constitute the glendonite pseudomorph, but provide no information on μm-size intergranular pores. We studied the nitrogen adsorption-desorption isotherms of untreated glendonite and ground powder of the same sample (Fig. 5). In particular, we examined the shape of the isotherms and the presence of hysteresis, which arises when the adsorbed nitrogen amount is not brought to the same level by the adsorption and desorption approach at a given equilibrium pressure or bulk concentration. Thus, it can be correlated with the structure of the mesopores. We also studied the hysteresis loops, which are correlated with the filling and emptying of the mesopores by capillary condensation. These loops are characterized by a lower (adsorption) branch obtained by the progressive addition of gas and an upper (desorption) branch obtained by the progressive withdrawal of gas. The shape of the loop provides useful qualitative information about the mesopore structure (Rouquerol et al. 2014).

During the 24-hour vacuum treatment at 300 °C we measured 0.03 and 1.30 % mass loss for the untreated and the powdered samples, respectively. According to IUPAC classification, the character of both isotherms is Type II, albeit mesopores (approximate range 2-50 nm) with negligible amount of micropores (diameter <2 nm) are present. Both isotherms rise sharply at low relative pressure ($p/p_0 <$ 0.1) consistent with the micropore filling of the precapillary condensation range. The adsorption is irreversible for both samples and the isotherms exhibit small hysteresis loops, which were attributed to the presence of mesopores (cumulative volume ~0.07 cm^3/g). We found no preferential pore size between 5 and 20 nm.

As a result of grinding, the gas uptake significantly increased, which is evidenced by the higher adsorbed nitrogen values of the isotherm in the whole p/p_0 range compared to the untreated sample. Accordingly, the specific surface area (5.78 m^2/g) and the pore volume (0.0704 cm^3/g) increased by ~50% and ~15% for the powdered sample (8.52 m^2/g and 0.0810 cm^3/g), respectively (Table 1). These results can be explained by (1) attrition of the material or (2) the opening of closed pores. Grinding the sample in an agate mortar results in a decrease in grain size and a concomitant increase in the specific surface area as reported by Tsai (2013). Furthermore, during grinding pores can be opened and become accessible to nitrogen. This second hypothesis is supported by the mesopore findings of the HAADF-STEM images (Fig. 2) and the relatively large mass loss of the powdered sample (1.30 mass %) compared to the untreated one (0.03 mass %) upon heating to 300°C under vacuum. However, air

239 moisture adhesion at the increased surface area of the powdered sample may also have contributed to
240 the mass loss during the pretreatment.
241 The nitrogen physisorption measurement shows that the surface area (5.78 m^2/g) and pore volume
242 (0.0704 cm^3/g) of our sample are only slightly larger than what is reported for natural calcite (4.05
243 m^2/g; 0.0240 cm^3/g) (Tsai 2013). However, the measured surface area of our glendonite sample is
244 significantly smaller than that of synthetic $CaCO_3$ prepared via a classical precipitation process (29.4
245 m^2/g) (Ashan 1992). Thus, we conclude that calcite crystals, the constituents of glendonite, are
246 characterized by low porosity.
247
248 *Possible relicts of the ikaite-to-calcite transformation in glendonite*
249 According to laboratory investigations (e.g., Swainson and Hammond 2003; Sánchez-Pastor et al.
250 2016; Purgstaller et al. 2017), the ikaite-to-calcite transformation is a relatively fast process (< 24
251 hours) even at low temperatures (10 °C). It may take longer than 24 hours in natural environments, but
252 the fact that the macroscopic ikaite morphology is commonly preserved (Sánchez-Pastor et al. 2016) is
253 consistent with a fairly rapid process.
254 Since the ikaite-to-calcite transformation is accompanied by a large (50 mass %) water loss, the
255 formation of abundant pores and entrapment of water in fluid inclusions, possibly along with the
256 development of interesting nanostructures can be expected. Our SEM and TEM results (Figs. 1 and 2)
257 show that in fact pores of μm to nm size are present and some of these pores contain water, in other
258 words, they represent fluid inclusions (Fig. 4). HAADF-STEM images indicate <100> aligned calcite
259 mesopores (Fig. 2), which may arise from a crystallographically oriented dehydration of the precursor
260 ikaite. TEM images also suggest that nanometer-size grains (10-40 nm) are common and {104} twins
261 occur (Figs. 3). Glendonite is characterized by high intergranular μm-size porosity. However, porosity
262 measurements of calcite, that build up glendonite pseudomorphs (Fig. 5, Table 1), reveal the
263 occurrence of relatively few mesopores (~0.07 cm^3/g) and a slightly increased pore volume compared
264 to natural calcite. Although these findings are consistent with the ikaite-to-calcite transformation, none
265 of them are uniquely diagnostic of this process. Pores and inclusion-hosted water are common in
266 secondary minerals (e.g., Demény et al. 2016a, b), twins are abundant in biogenic calcite (e.g., Larsson
267 and Christy 2008) and the porosity values of calcite, the constituent of glendonite, are consistent with a
268 relatively low-porosity material. Our results therefore suggest the transformation of ikaite to calcite
269 leaves behind very few structural relicts in the glendonite pseudomorphs.
270

IMPLICATIONS

The glendonite morphology remains the most reliable feature to identify calcite derived via transformation of ikaite. During this process practically all the water leaves the system. As a result, the geochemical composition can presumably be altered similar to what was reported for the ACC-to-calcite recrystallization (Demény et al. 2016b). Thus, the reliability of proxy data derived from glendonite may be affected. In particular, such diagenetic processes will likely have affected the O-isotopic composition of glendonites in older geological rocks that experienced elevated burial temperatures. In the case of samples from the Quaternary period ^{230}Th/U ages may be influenced by the likely loss of U during dewatering, resulting in problematic chronologies. These findings have implications for the emerging research field of cryogenic caves carbonates, which are commonly associated with the presence of permafrost (Žák et al. 2012, 2018). Detailed mineralogical and geochemical studies are required to fully assess the possible role of ikaite as a precursor of cryogenic calcite in cases where no glendonite pseudomorphs are present.

ACKNOWLEDGMENTS

The project was supported by the bilateral grants 2019-2.1.11-TÉT-2019-00016, NKFIH ANN134433, FWF I027070 and FWF FI5050. We are grateful to the staff and for use of the TEM facility at the University of Pannonia, established using grant no. GINOP-2.3.3-15-2016-0009 from the European Structural and Investments Funds. P.N. acknowledges financial support from the Hungarian National Research, Development and Innovation Office (projects FK123871 and NKFIH-872), the Eötvös Loránd Research Network (NANOCARB project, SA-41/2021) as well as the János Bolyai Research Scholarship and the ÚNKP-20-5-PE-7 New National Excellence program of the Ministry for innovation and technology.

References cited

Ashan, T. (1992) The surface properties of pure and modified precipitated calcium carbonate by adsorption of nitrogen and water vapor. Colloids and Surfaces**,** 64, 167- I76.

Barrett, E.P., Joyner, L.G., Halenda, P.P. (1951) The determination of pore volume and area distributions in porous substances. I. Computations from nitrogen isotherms. Journal of the American Chemical Society, 73 (1), 373-380.

Barber, D.J., Reeder, R.J., and Smith, D.J. (1985) A TEM microstructural study of dolomite with curved faces (saddle dolomite). Contributions to Mineralogy and Petrology, 91, 82–92.

Bazarova, E.P., Kononov, A.M., Gutareva, A.M., and Nartova, N.V. (2014) Characteristics of cryogenic mineral formations of Okhotnichiya cave at Pre-Baikal areas (Irkutsk region). Earth's Cryosphere, 18 (3). 67 – 76.

Boch, R., Dietzel, M., Reichl, P., Leis, A., Baldermann, A., Mittermayr, F., and Pölt, P. (2015) Rapid ikaite ($CaCO_3 \cdot 6H_2O$) crystallization in a man-made river bed: hydrogeochemical monitoring of a rarely documented mineral formation. Applied Geochemistry 63, 366–379.

Brooks, R., Clark, L.M., and Thurston, E.F. (1950) Calcium carbonate and its hydrates. Philosophical Transactions of the Royal Society of London Series A, 243, 145-167.

Brunauer, S., Emmet, P.H., and Teller E. (1938) Adsorption of gases in multimolecular layers. Journal of the American Chemical Society, 60 (2), 309-319.

Council, Te., and Bennett, P.e. (1993) Geochemistry of ikaite formation at Mono Lake, California: implications for the origin of tufa mounds. Geology, 21, 971-974.

De Lurio, J.L., and Frakes, L.A. (1999) Glendonites as a paleoenvironmental tool: Implications for early Cretaceous high latitude climates in Australia. Geochimica et Cosmochimica Acta, 633, 1039-1048.

Demichelis, R., Raiteri, P., and Gale, J.D. (2014) Structure of hydrated calcium carbonates: A first principles study. Journal of Crystal Growth, 401, 33-37.

Demény, A., Czuppon, Gy., Kern, Z., Leél-Őssy, Sz., Németh, A., Szabó, M., Tóth, M., Wu, Ch-Ch., Shen Ch-Ch., Molnár, M., Németh, T., Németh P., and Óvári, M. (2016a) Recrystallization-induced oxygen isotope changes in inclusion hosted water of speleothems - paleoclimatological implications. Quaternary International, 415, 25-32.

Demény, A., Németh, P., Czuppon, Gy., Leél-Őssy, Sz., Szabó, M., Judik, K., Németh, T., and Stieber, J. (2016b) Formation of amorphous calcium carbonate in caves and its implications for speleothem research, Scientific Reports, 6, 39602. DOI: 10.1038/srep39602.

Dublyansky, Y., Moseley, G. E., Lyakhnitsky, Y., Cheng, H., Edwards, R. L., Scholz, D. et al. (2018) Late Palaeolithic cave art and permafrost in the Southern Ural. Scientific Reports, 8(1), 12080. DOI: 10.1038/s41598-018-30049-w.

Field, L. P., Milodowski, A. E., Shaw, R.P., Stevens, L. A., Hall, M. R., Kilpatrick, A., Gunn, J., Kemp, S. J., Ellis, M. A. (2017) Unusual morphologies and the occurrence of pseudomorphs after ikaite ($CaCO_3 \cdot 6\ H_2O$) in fast growing, hyperalkaline speleothems. Mineralogical Magazine, 81(3), 565–589.

Greinert, J. and Derkachev, A. (2004) Glendonites and methane derived Mg-calcites in the Sea of Okhotsk, Estern Siberia: implications of a venting-related ikaite/glendonite formation. Marine

337 Geology, 204, 129-144.
338 Hu, Y.B., Wolf-Gladrow, D.A., Dieckmann, G.S., Völker, C., and Nehrke, G. (2014) A laboratory
339 study of ikaite ($CaCO_3$*$6H_2O$) precipitation as a function of pH, salinity, temperature and
340 phosphate concentration. Marine Chemistry, 162, 10–18.
341 Huggett, J. M., Schultz, B. P., Shearman, D. J., and Smith, A. J. (2005) The petrology of ikaite
342 pseudomorphs and their diagenesis. Proceedings of the Geologists' Association, 116(3-4), 207–
343 220.
344 Jansen, J.H.F., Woensdregt, E.F., Kooistra, M.J., and Van Der Gaast, S.J. (1987) Ikaite pseudomorphs
345 in the Zaire deep sea fan: an intermediate between calcite and porous calcite. Geology, 15, 245-
346 248.
347 Larsen, D. (1994) Origin and paleoenvironmental significance of calcite pseudomorphs after ikaite in
348 the Oligocene Creede Formation, Colorado. Journal of Sedimentary Research, A64, 593-603.
349 Larsson, A-K. and Christy, A.G. (2008) On twinning and microstructures in calcite and dolomite.
350 American Mineralogist, 93, 103–113.
351 Németh, P. (2021) Diffraction features from $(10\bar{1}4)$ calcite twins mimicking crystallographic ordering.
352 Minerals, 11 (7), 720. https://doi.org/10.3390/min11070720.
353 Nyírő-Kósa, I, Rostási, Á., Bereczki-Tompa, É., Cora, I., Koblar, M., Kovács, A., and Pósfai, M.
354 (2018) Nucleation and growth of Mg-bearing calcite in a shallow, calcareous lake. Earth and
355 Planetary Science Letters, 496 , 20-28.
356 Onac, B.P., Wynn, J.G., and Citterio, M. (2011) Ikaite in the Scari¸soara Ice Cave (Romania): origin
357 and significance, Geophysical Research Abstracts, 13, EGU2011-5188.
358 Pauly, H. (1963) 'Ikaite', a new mineral from Greenland. Arctic Research, 16, 263-279.
359 Pelouze, M.J. (1865) Sur une combination nouvelle d'eau et de carbonate de chaux. Chemical Review,
360 60, 429-43.
361 Popov, L.E., Álvaro, J.J., Holmer, L.E., Bauert, H., Pour, M.G., Dronov, A.V., Lehnert, O., Hints, O.,
362 Männik, P., Zhang Z and Zhang Z. (2019) Glendonite occurrences in the Tremadocian of Baltica:
363 first Early Palaeozoic evidence of massive ikaite precipitation at temperate latitudes. Scientific
364 Reports, 9, 7205
365 Purgstaller, B., Dietzel, M., Baldermann, A., Mavromatis, V. (2017) Control of temperature and
366 aqueous Mg^{2+}/Ca^{2+} ratio on the (trans-)formation of ikaite. Geochimica et Cosmochimica Acta
367 217, 128–143.
368 Reeder, R. J. (1992) Carbonates: Growth and alteration microstructures. Reviews in Mineralogy 27,
369 381–424.

Reeder, R.J. and Wenk, H.R. (1979) Microstructures in low-temperature dolomites. Geophysical Research Letters, 6, 77–80.

Rouquerol, F, Rouquerol, J., Sing, K.S.W., Llewellyn, P. and Maurin, G. (2014) Adsorption by Powders and Porous Solids Principles, Methodology and Applications, 2nd ed., Academic Press

Sánchez-Pastor, N., Oehlerich, M., Astilleros, J.M., Kaliwoda, M., Mayr, C.C., Fernández-Díaz, L., and Schmahl, W.W. (2016) Crystallization of ikaite and its pseudomorphic transformation into calcite: Ramen spectroscopy evidence. Geochimica et Cosmochimica Acta, 175, 271-281.

Suess, E., Balzer, W., Hesse, K.F., Muller, P.J., and Wefer, G. (1982) Calcium carbonate hexahydrate from organic-rich sediments of the Antarctic Shelf: Precursor of glendonites. Science, 1216, 1128-1131.

Swainson, I.P. and Hammond, R.P. (2001) Ikaite, $CaCO_3.6H_2O$: Cold comfort for glendonites as palaeothermometers. American Mineralogist, 86(11–12), 1530–1533.

Swainson, I.P. and Hammond, R.P. (2003) Ikaite, $CaCO_3 \cdot 6H_2O$: Hydrogen bonding in ikaite, $CaCO_3.6H_2O$. Mineralogical Magazine, 67 (3), 555-562.

Tollefsen, E., Balic-Zunic, T., Mörth, C.M., Brüchter, V., Lee, C.C., and Skelton, A. (2020) Ikaite nucleation at 35 °C challenges the use of glendonite as a paleotemperature indicator. Scientific Reports, 10, 8141.

Tsai, W.T. (2013) Microstructural characterization of calcite-based powder materials prepared by planetary ball milling, Materials, 6, 3361-3372.

Žák, K., Richter, D.K., Filippi, M., Živor, R., Deininger, M., Mangini, A., and Scholz, D. (2012) Coarsely crystalline cryogenic cave carbonate - a new archive to estimate the Last Glacial minimum permafrost depth in Central Europe. Climate of the Past, 8(6), 1821–1837.

Žák, K., Onac, B.P., Kadebskaya, O., Filippi, M., Dublyansky, Y., and Luetscher, M. (2018) Cryogenic Mineral Formation in Caves, in: Perşoiu, A., Lauritzen, S.-E. (Eds.), Ice caves, Elsevier, Amsterdam.

This is the peer-reviewed, final accepted version for American Mineralogist, published by the Mineralogical Society of America.
The published version is subject to change. Cite as Authors (Year) Title. American Mineralogist, in press.
DOI: https://doi.org/10.2138/am-2022-8162. http://www.minsocam.org/

Figure and table captions

Figure 1: Morphology and porosity of glendonite from Victoria cave. a) Drusy glendonite aggregate composed of tetragonal pyramids. b) and c) SEM images of glendonites forming hollow (sheath-like) canted tetragonal pyramids, with the interior void filled with clumpy material. d) Aggregated grains with μm to subμm-size pores (magnified from b). e) Rare euhedral calcite crystals (magnified from d). f) Enlargement of c). g) Flaky calcite crystals on the surface of outer layer of the sheath-like pyramid underlain by small equant anhedral crystals; note intergranular porosity (magnified from f).

Figure 2: Mesopores and twins in nanocrystalline aggregated calcite formed from ikaite. a) HAADF-STEM image and SAED pattern (taken from the area marked by the white arrow) of a $[10\bar{1}2]$ elongated grain with <100> oriented mesopores. b) Magnified image from a). White line marks a $(10\bar{1}4)$ twin plane. EDS data (insert) shows the characteristic X-ray lines of $CaCO_3$. c) and d) Structure models of ikaite and calcite viewed along [010] and [0110], respectively.

Figure 3. $(10\bar{1}4)$ calcite twins and overlapping nanograins in glendonite. a) HRTEM image of a ~10 nm size $(10\bar{1}4)$ twin domain within the calcite matrix along [0110]. White arrows of the corresponding SAED pattern (right upper corner) point to extra reflections arising from the twin domains. b) HRTEM image of a $(10\bar{1}4)$ twin and Moire patterns. Moire fringes (marked by a black circle) indicate ~10-20 nm-sized overlapping nanograins. The FFT calculated from the image reveals $(10\bar{1}4)$ twin reflections (white arrows) and satellites arising from the superposition of the nanograins (indicated by the white circle). c) HRTEM image of glendonite along [0110]. Moire fringes (marked by a white arrow) indicate ~40 nm-sized thin overlapping nanograins. d) Area magnified from a) and FFT calculated from the image reveals satellites arising from the superposition of the nanograins (indicated by the white circles). The overlapping grains are rotated by ~ 12° with respect to each other.

Figure 4. FTIR absorption spectra (arbitrary units) of multiple glendonite grains from Victoria cave using different treatments and measurement techniques. ‘T’ are measurements of untreated grains in transmission mode. ‘T – dry’ refers to measurements in transmission mode of an untreated sample that was dried at 105°C for 24 hours before analysis. Spectra labelled ‘T – D_2O treated’ were measured on grains soaked in D_2O for 48 hours. ‘ATR’ refers to an untreated sample in attenuated total reflectance

mode. 'D_2O pure' shows the pure D_2O reagent used in the treatment measured as a thin film between two BaF_2 optical windows. Vertical dashed lines mark characteristic calcite absorption bands. Grey bars cover the range of absorption typical for molecular H_2O and D_2O. In order to highlight the interesting features the spectra were scaled and vertically offset.

Figure 5. Nitrogen adsorption isotherms of untreated and powdered glendonite. Full and open symbols correspond to adsorption and desorption branches, respectively.

Table 1. Summary of porosity measurements.

	Untreated glendonite	Powdered glendonite
Mass loss during pretreatment (mass %)	0.03%	1.3%
Total pore volume (cm^3/g)	$\sim 7.04*10^{-2}$	$\sim 8.10*10^{-2}$
Specific surface area (m^2/g)[1]	~5.78	~8.52
Mesopore diameter (nm)[2]	5-20	5-20
Cumulative mesopore volume (cm^3/g)[2]	$\sim 6.99*10^{-2}$	$\sim 8.0*10^{-2}$

[1] calculated by BET method (Brunauer et al. 1938)

[2] calculated for adsorption branch by the BJH method (Barrett et al. 1951)

This is the peer-reviewed, final accepted version for American Mineralogist, published by the Mineralogical Society of America.
The published version is subject to change. Cite as Authors (Year) Title. American Mineralogist, in press.
DOI: https://doi.org/10.2138/am-2022-8162. http://www.minsocam.org/

Fig. 1

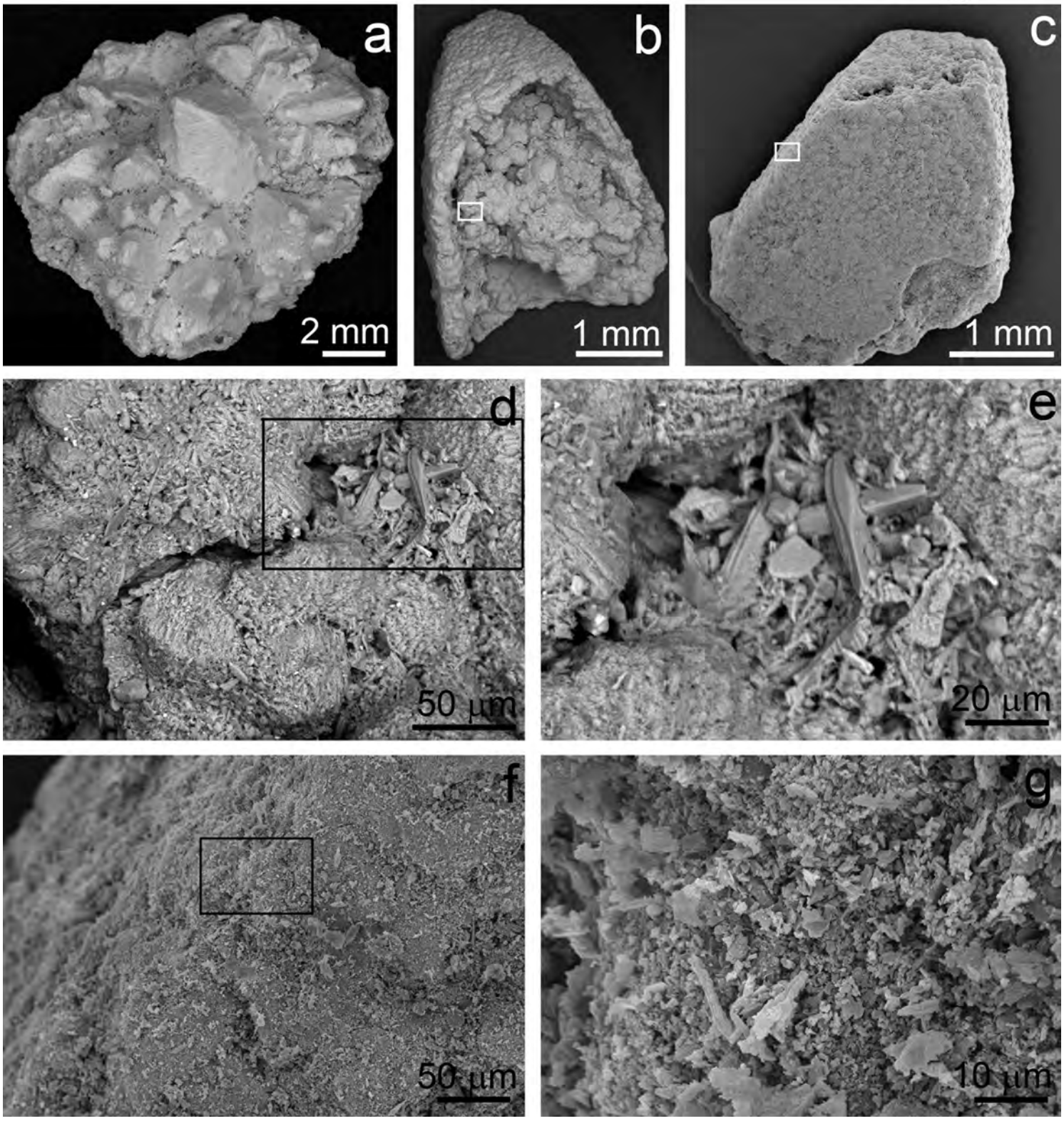

This is the peer-reviewed, final accepted version for American Mineralogist, published by the Mineralogical Society of America.
The published version is subject to change. Cite as Authors (Year) Title. American Mineralogist, in press.
DOI: https://doi.org/10.2138/am-2022-8162. http://www.minsocam.org/

Fig. 2

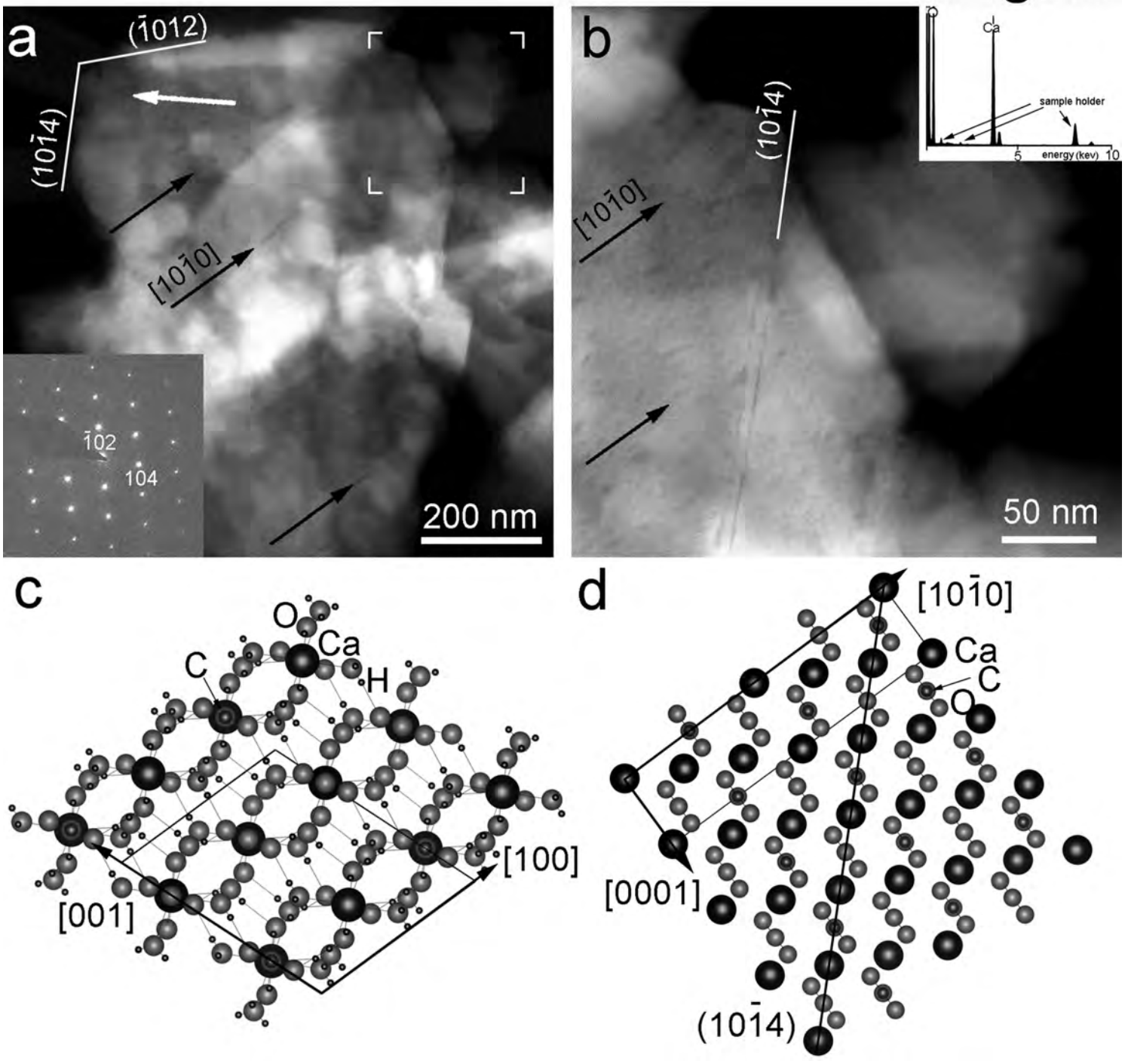

This is the peer-reviewed, final accepted version for American Mineralogist, published by the Mineralogical Society of America.
The published version is subject to change. Cite as Authors (Year) Title. American Mineralogist, in press.
DOI: https://doi.org/10.2138/am-2022-8162. http://www.minsocam.org/

Fig. 3

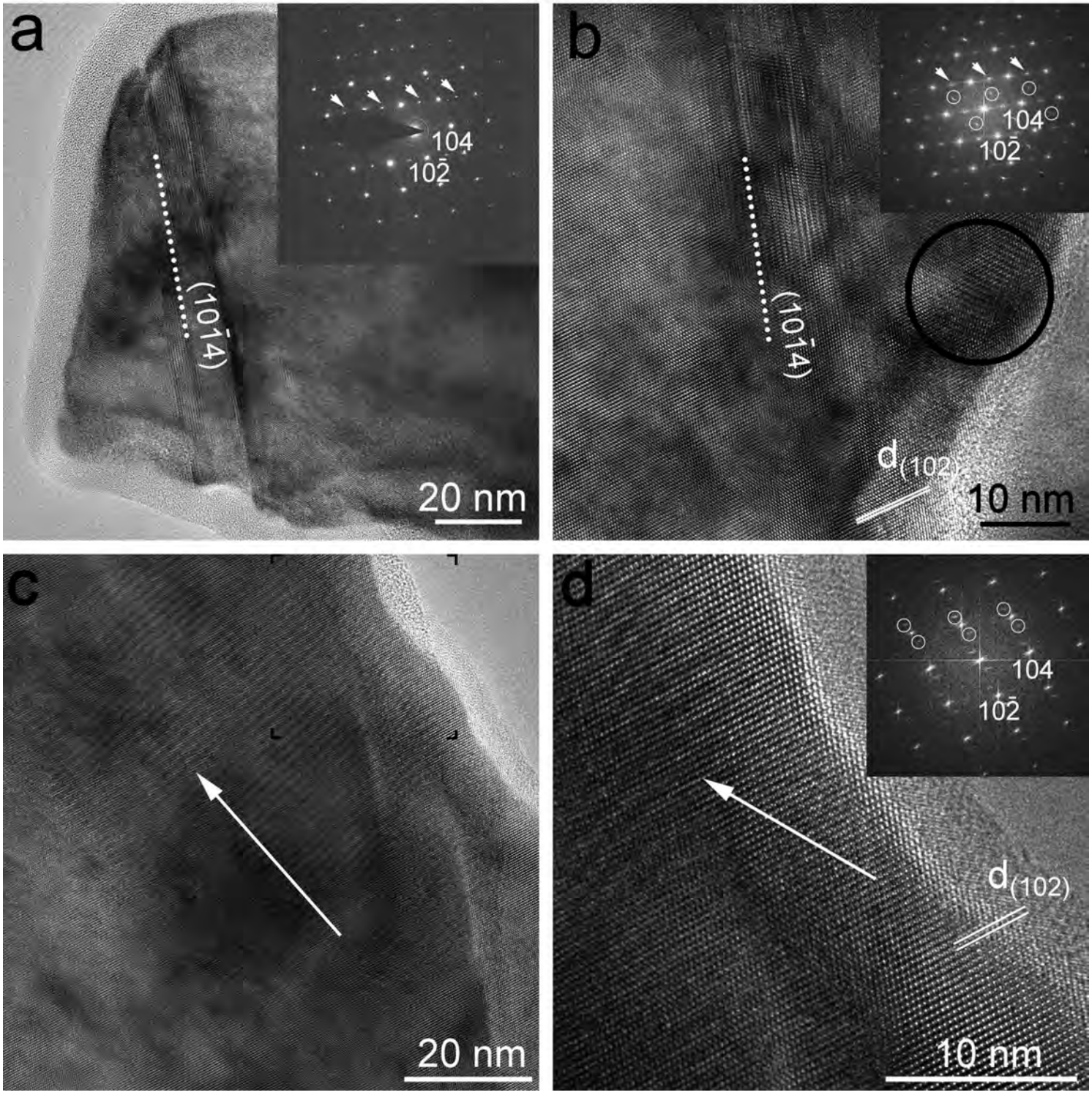

Fig. 4

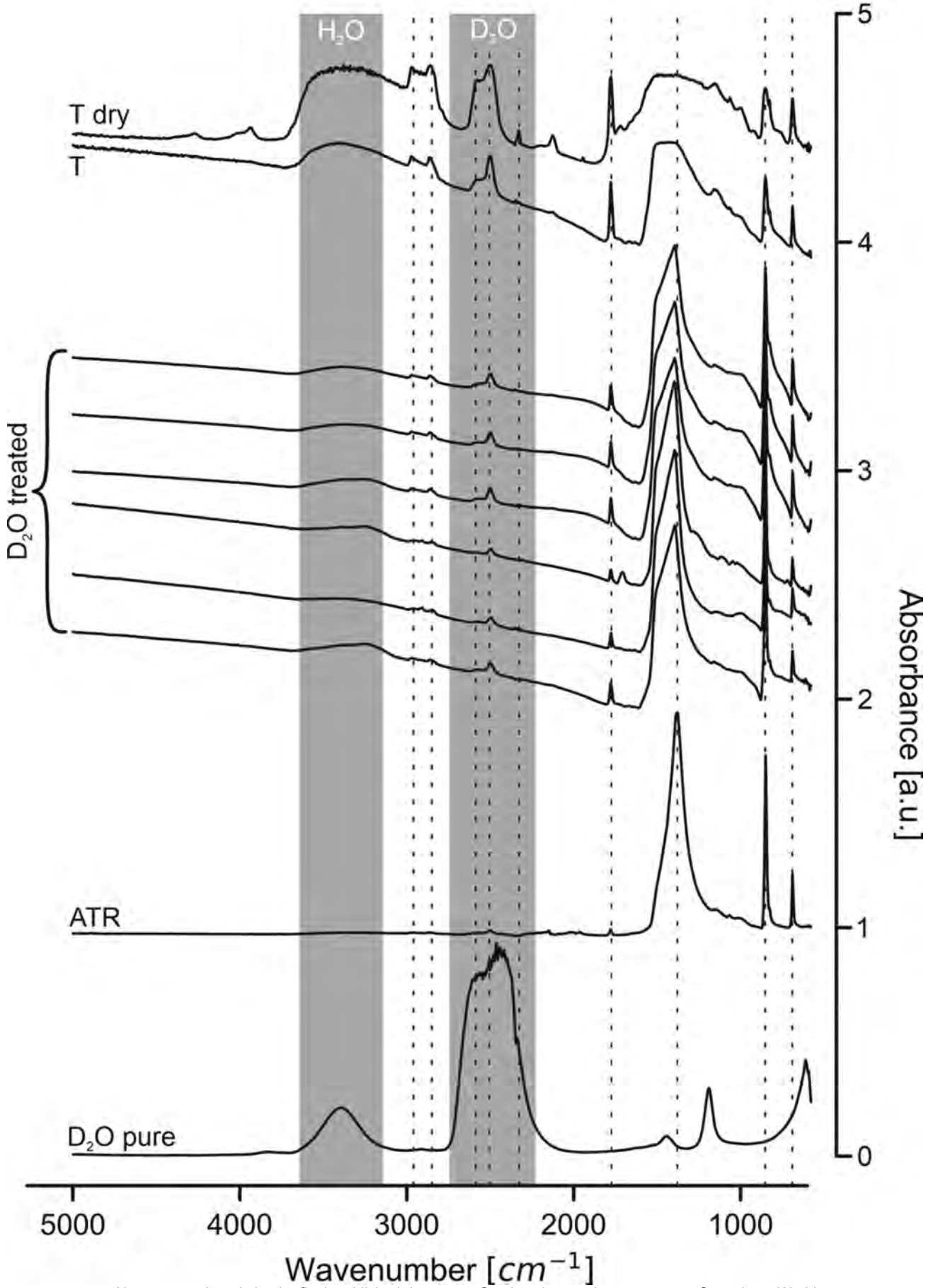

This is the peer-reviewed, final accepted version for American Mineralogist, published by the Mineralogical Society of America.
The published version is subject to change. Cite as Authors (Year) Title. American Mineralogist, in press.
DOI: https://doi.org/10.2138/am-2022-8162. http://www.minsocam.org/

Fig. 5

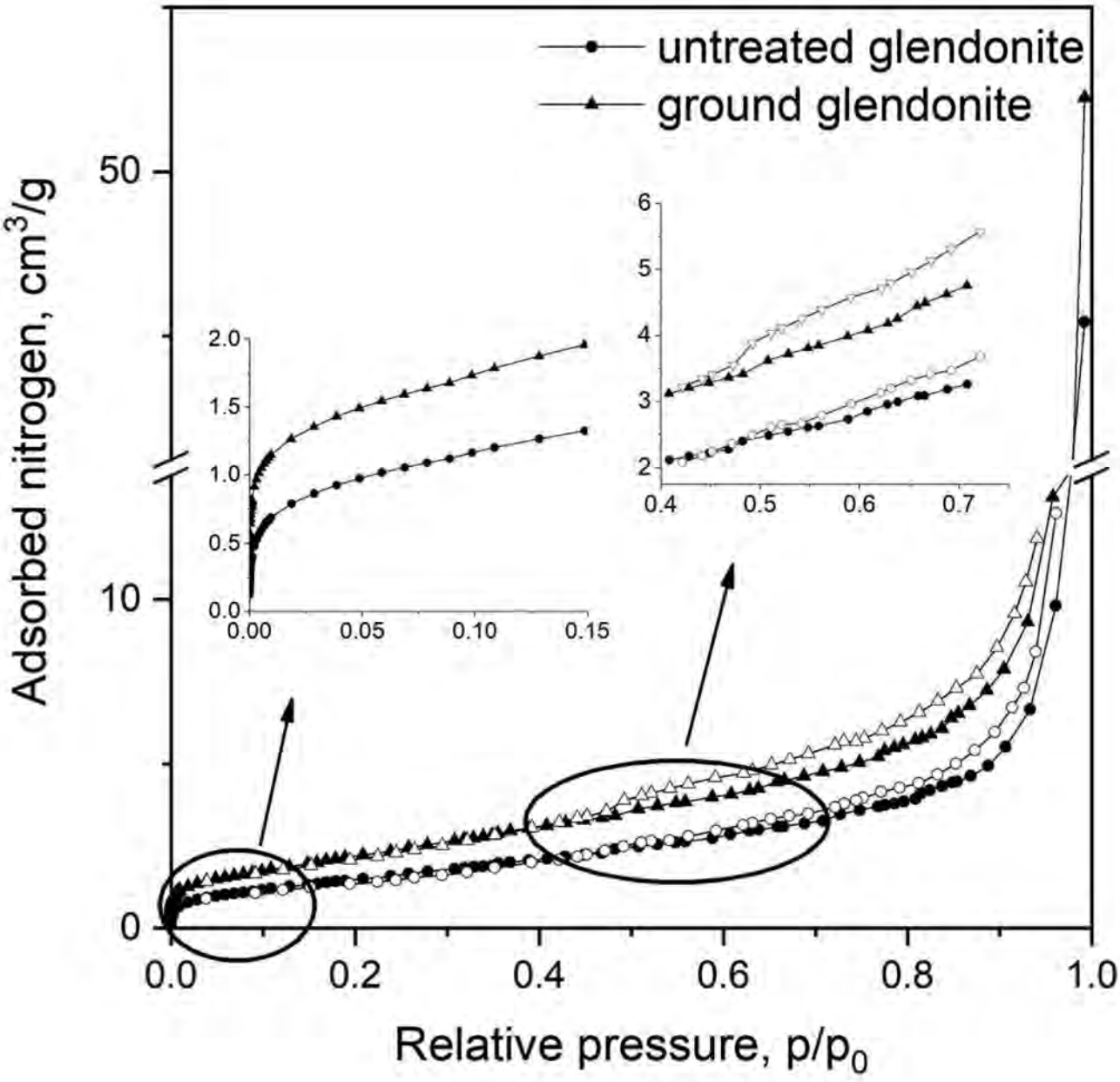

This is the peer-reviewed, final accepted version for American Mineralogist, published by the Mineralogical Society of America.
The published version is subject to change. Cite as Authors (Year) Title. American Mineralogist, in press.
DOI: https://doi.org/10.2138/am-2022-8162. http://www.minsocam.org/

Table 1. Summary of porosity measurements.

	Untreated glendonite	Powdered glendonite
Mass loss during pretreatment (mass %)	0.03%	1.3%
Total pore volume (cm^3/g)	~$7.04*10^{-2}$	~$8.10*10^{-2}$
Specific surface area (m^2/g)[1]	~5.78	~8.52
Mesopore diameter (nm)[2]	5-20	5-20
Cumulative mesopore volume (cm^3/g)[2]	~$6.99*10^{-2}$	~$8.0*10^{-2}$

[1] calculated by BET method (Brunauer et al. 1938)

[2] calculated for adsorption branch by the BJH method (Barrett et al. 1951)